



Full Length Article

Photocatalytic and eco-emission applications of green synthesized ZnO-CB nanoparticles

J.P. Shubha^{a,*}, B. Roopashree^b, N.V. Sushma^c, K. Kiran^d, R. Ravikumar^d, Mufsir Kuniyil^e, Mohammed Rafi Shaik^e, Mujeeb Khan^e, Syed Farooq Adil^{e,**}^a Department of Chemistry, Sri Jayachamarajendra College of Engineering, JSS Science & Technology University, Mysuru 570006, India^b Department of Chemistry, JSS Academy of Technical Education, Dr. Vishnuvardhan Road, Bengaluru 560060, India^c Department of Chemistry, Don Bosco Institute of Technology, Mysore Road, Bangalore 560074, India^d Department of Mechanical and Automobile Engineering, School of Engineering and Technology, CHRIST University, Bengaluru 560074, India^e Department of Chemistry, College of Science, King Saud University, P.O. Box 2455, Riyadh 11451, Saudi Arabia

ARTICLE INFO

Keywords:

ZnO-CB
Calyxes of brinjal
Dye degradation
Photocatalysis
Milletia pinnata oil methyl ester
Green emissions

ABSTRACT

Herein, we report the synthesis of ZnO nanoparticles (ZnO-CB NPs) by employing the solution combustion method using an aqueous extract of brinjal calyxes as fuel. Characterization techniques, such as X-ray diffraction (XRD), Fourier transform Infrared spectroscopy (FTIR), UV-visible spectroscopy, and Scanning electron microscopy (SEM), were used to investigate the structural, optical, and morphological properties of synthesized nanoparticles, respectively. Highly porous hexagonal crystalline ZnO-CB NPs with less than 7 nm particle size were obtained. The photocatalytic performance of synthesized material is measured with Malachite green (MG), Basic brown 1 (BB1), and Acid orange 36 (AO36) as benchmark dyes. It showed that the synthesized material worked effectively under pH 10 with UV light irradiation. The synthesized ZnO-CB NP shows good removal effectiveness of the MG, BB1, and AO36 dyes with 99.3 %, 99.6 %, and 99.5 %, respectively, which can be promising photocatalysts for ecological applications such as wastewater remediation. Further, the synthesized ZnO-CB NP was used as blends in the methyl ester of *Milletia pinnata* oil (MPME), which is blended 20 % with commercial diesel (MPME20). The synthesized ZnO-CB NP was added to the MPME20 in varying amounts to ascertain its effects on the quality of emissions of various greenhouse gases such as hydrocarbons, CO_x, and NO_x. Moreover, brake thermal efficiency (BTHE) and brake-specific fuel consumption (BSFC) were studied for the blends. The blend MPME20 with 25 mg of ZnO-CB NP, i.e., MPME20-25 mg, ZnO-CB, displays the best performance and reduced emissions.

1. Introduction

Irreparable disposal of highly stable compounds such as dyes, drugs, plastics, pesticides, heavy metals, etc., from different sources such as agriculture, industries, and urban cities has a significant negative impact on the environment (Zollinger 2003; Fosso-Kankeu et al., 2020). These harmful organic dyes have a major unconstructive blow on the environment. Numerous processes, including chemical oxidation, adsorption, precipitation, ion exchange, biological, reverse osmosis, and photocatalysis, are used to break down these harmful dyes (Zollinger, 2003). These procedures are likely to be rejected by effluent treatment processes because they are ineffective and expensive. The above-

mentioned challenges for the degradation of dyes present in effluents must thus be reduced. This calls for cost-effective and environmentally safe alternative processes.

One of the optimum methods for the degradation of hazardous dyes in effluent water with the use of semiconductor-based photocatalysts is the advanced oxidation process, which has been suggested thus far (Pouretedal et al., 2009; Alharthi et al., 2020). Due to their high efficiency, environmentally encouraging nature, and affordability, these semiconductor photocatalysts are regularly used (Mills et al., 1993; Lavand and Malghe 2015; Hassaan et al., 2017; Navarro et al., 2017; Natarajan et al., 2018a, 2018b; Pirhashemi et al., 2018; Belver et al., 2019; Di et al., 2019). Modern researchers have been progressively more

* Corresponding author.

** Corresponding author.

E-mail addresses: shubhapanesh@gmail.com (J.P. Shubha), sfadil@ksu.edu.sa (S. Farooq Adil).<https://doi.org/10.1016/j.jksus.2024.103373>

Received 20 February 2024; Received in revised form 25 July 2024; Accepted 26 July 2024

Available online 29 July 2024

1018-3647/© 2024 The Author(s). Published by Elsevier B.V. on behalf of King Saud University. This is an open access article under the CC BY license (<http://creativecommons.org/licenses/by/4.0/>).

interested in the expansion of effective green chemistry processes for the production of metal oxide nanoparticles. There are many potential methods for the successful production of metal oxide NPs (Mills et al., 1993; Capek, 2006; Lavand and Malghe, 2015; Hassaan et al., 2017; Navarro et al., 2017; Pirhashemi et al., 2018; Singh et al., 2018; Belver et al., 2019; Di et al., 2019). Several nanostructured metal oxides can have their magnetic, optical, and electrical properties altered by altering the synthesis and processing conditions (Thema et al., 2015; Thovhogi et al., 2016). They may, therefore, have characteristics related to a number of industrial applications, including catalysts, battery cathodes, gas sensors, magnetic materials, antibacterial (Singh et al., 2018), etc.

Some transition metal oxides, including NiO, TiO₂ etc., nanoparticles show potential as antioxidants (Abbasi et al., 2019), photocatalysts (Dooley et al., 1994), angiogenesis inhibitors (Kumar et al., 2021), and electrochemical sensors (Amin et al., 2019). In the current era, doped transition metal oxide semiconductors have received a lot of attention because of their increased catalytic properties (Al Boukhari et al., 2020).

Several varieties of plant and fruit extracts were employed for the biosynthesis of ZnO NPs, namely, *Salvadoraoleoides*, *Echinacea spp.*, *Boswelliaovalifoliolata*, and *Ocimumamericanum* (Supraja et al., 2016; Padalia et al., 2017; Attar and Yapaoz, 2018; Narendra Kumar et al., 2019), which were utilized as photocatalytic agents for various organic dyes, such as methylene blue (MB) dye, and 88 % degradation was obtained in 140 min. Eco-friendly ZnO-CB-NPs were used as photocatalytic agents for many organic dyes, such as methylene blue (MB) dye, which degraded (88 %) in 140 min (Supraja et al., 2016). Padalia et al., and his team degraded up to 86 % in 180 min (Padalia et al., 2017). The photocatalytic assessment proved the ZnO NPs achieved 100 % elimination of MB dye at 60 min exposure, and 85 and 92 % degradation of methyl orange (MO) and Rhodamine B (RhB), respectively, at 180 min (Karaköse and Çolak 2018).

In order to achieve high photo-decomposition activity over three organic chronic dyes, malachite green (MG), basic brown 1 (BB1), and acid orange 36 (AO36), it is attempted to synthesize ZnO-CB NPs as photocatalyst in a cost-effective and environmentally friendly combustion method using aqueous extract of calyces of brinjal as fuel as illustrated in Scheme 1A. Under the illumination of various light sources, the synthesized ZnO-CB NPs are used as a photocatalyst to remove dyes from an aqueous solution. Furthermore, the impact of several catalytic parameters on the photocatalytic degradation of MG, BB1, and AY36 dyes is also examined, including irradiation time, dye concentration, photocatalyst quantity, and pH value. The ZnO-CB NPs photocatalyst demonstrated outstanding photocatalytic performance for the degradation of MG, BB1, and AO36 dyes under UV light irradiation, as shown by the photocatalytic data. Under identical conditions, 99.6 % and 99.3 % of MG and BB1 dyes are degraded within 100 min, respectively where,

as 99.5 % of AO36 degraded in 120 min.

Biodiesel, which is derived from green sources, is *trans*-esterified for structural modification and is suggested as an alternative as it has more energy safety, a variety of sources, and considerable carbon emission decrease (Javed et al., 2016; Prabu and Anand 2016; Esfe et al., 2018; Hasannuddin et al., 2018; Devarajan et al., 2019; Desantes et al., 2020; Kumar et al., 2020; Soudagar et al., 2020; Elumalai et al., 2021; Soudagar et al., 2021). Although biodiesel has garnered attention in recent study, it is not without limitations, such as increased NO_x emissions, lower energy output, and increased fuel consumption. According to studies, there are plenty of *Millettia pinnata* trees in different parts of India (Desantes et al., 2020), and transesterification yields an 81 % yield of biodiesel (MPME) from *Millettiapinnata* oil.

Fuel combustion efficiency is significantly influenced by ZnO nanoparticles, which assist in the breakdown of complex hydrocarbons and catalyze complete combustion (Yusof et al., 2020; Ampah et al., 2022). ZnO nanoparticles possess "oxygen buffering capability", which guarantees that there is enough oxygen available for combustion, especially in lean fuel mixtures—and increases the efficiency of the fuel. Furthermore, by changing the kinetics of combustion, ZnO nanoparticles can aid in the reduction of harmful gases such as NO_x and CO_x in the emissions (Rajak et al., 2023; Suhel et al., 2023). Hence, it is worth studying the effect of green synthesized ZnO NPs and how the synthetic protocol employed affects the catalytic performance. Therefore, the catalytic property of ZnO-CB NPs is tested in the enhancement of the fuel properties by adding different proportions of catalyst in MPME and diesel blends. The emission analysis of the engine is performed using an exhaust emission analyzer.

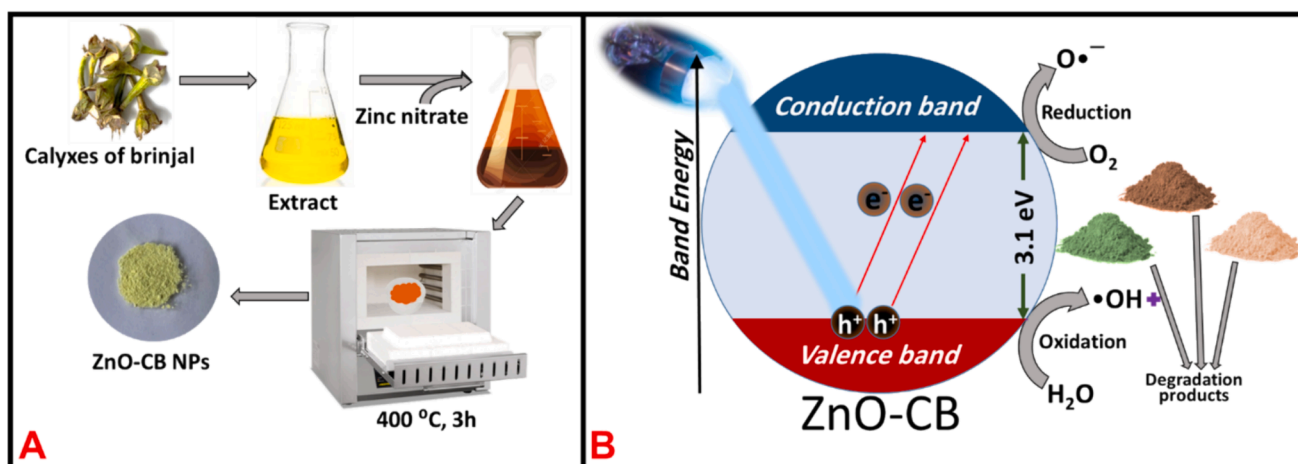
2. Materials and methods

2.1. Materials

Analytical-grade zinc nitrate hexahydrate (Zn(NO₃)₆·6H₂O) (Sigma-Aldrich), malachite green (Sigma-Aldrich), basic brown1 (Sigma-Aldrich), and acid yellow 36 (gift sample) are used without further purification. Double-distilled water is used throughout the work.

2.2. Preparation of aqueous extract of calyces of brinjal

Just separated calyces from brinjal are washed with distilled water, dried, and about 100 g are boiled in 150 mL distilled water until the volume is reduced to 50 mL. Then, they are filtered, cooled, and used for the synthesis of ZnO-CB photocatalyst.



Scheme 1. (A) Graphical representation of synthesis of ZnO-CBNPs, and (B) A proposed mechanism for the degradation of dyes.

2.3. Synthesis of zinc oxide nanoparticles (ZnO-CB NPs) photocatalyst using extract of calyces of brinjal

The synthesis is carried out using zinc nitrate (0.7355 g) and an aqueous extract of brinjal calyces. Zinc nitrate is dissolved in 5 mL of distilled water and mixed with 4 mL of brinjal calyces aqueous extract with constant stirring until a thick mass is obtained. The thick mass is kept in a preheated muffle furnace for 15 min at 400 ± 10 °C, followed by calcination at the same temperature for 3 h. The obtained product (labeled as ZnO-CB NPs) is stored in airtight vials.

2.4. Photocatalytic experimentation

The experimental setup consists of a spherical-shaped glass bowl of 250 ml capacity, a magnetic stirrer (Make: Remi), a magnetic bit, and an electric connection. The speed of the magnetic stirrer is set at 450 rpm. 5, 10, 15, and 20 mg of ZnO-CB in 100 mL of aqueous dye solution at 3, 6, 9, and 12 ppm are taken for degradation experiments. These solutions are aerated by keeping in the dark for 40 min. Then, solutions are kept under UV-light by constant stirring at intervals of 30 min; nearly 3 mL of the aqueous mixture is collected from the reaction solution and subjected to centrifugation. The clear solution is withdrawn and transferred to the cuvette, and absorption is measured with a UV-visible spectrophotometer (Labman: LMSP-UV1900).

2.5. Blending of MPME

To further the above catalytic studies, ZnO-CB is employed as a blend. MPME is mixed with commercial diesel at 20 % by volume. This blend is termed MPME20, as standardized by earlier studies (McCormick et al., 2006). Furthermore, this blend is further combined with varying amounts of ZnO-CB NPs, i.e., 25 mg and 40 mg, which are termed MPME20 + 25 mg ZnO-CB and MPME20 + 40 mg ZnO-CB, respectively, using an ultrasonication bath, and subsequently used as fuels for engine experiments. Similar blends are created by employing the chemically synthesized ZnO-CB NPs, i.e., ZnO-CB, and the blends are labeled MPME20 + 25 mg ZnO-CB and MPME20 + 40 mg ZnO-CB, which contain varying amounts of ZnO-CB NPs, i.e., 25 mg and 40 mg, respectively.

3. Results and discussion

3.1. Characterizations of ZnO-CB NPs

3.1.1. Powder X-ray diffraction

ZnO-CB NPs are synthesized using an extract of calyces of brinjal utilizing green protocol. In order to obtain the physical and chemical

properties of the synthesized nanoparticles, various techniques are employed. The crystalline nature and the crystalline size are estimated by X-ray diffraction spectroscopy. Fig. 1A displays the XRD pattern of the synthesized ZnO-CB NPs, which depicts a highly crystalline nature. All the diffracted peaks are identified as matching with the hexagonal wurtzite structure of ZnO, which is in accordance with the JCPDS Card No. 36-1451. The peaks present at 2θ values of 31.6° , 34.3° , 36.1° , 47.4° , 56.4° , 62.8° , 66.3° , 67.8° , and 68.8° are indexed to (100), (002), (101), (102), (110), (103) and (112) lattice planes, respectively (Bououdina et al., 2017). The average crystallite size (D) of the ZnO-CB NPs is calculated using the Scherer equation (Eq. (1)) as 6.9 ± 0.89 nm, and the lattice constants are $a = 0.33$ nm and $c = 0.52$ nm.

$$D = \frac{k\lambda}{\beta \cos\theta} \quad (1)$$

where k – constant, λ – wavelength of X-rays, β – line broadening at half the maximum intensity, θ – Bragg angle.

3.1.2. FTIR analysis

Fig. 1B depicts the transmittance spectrum of ZnO-CB NPs formed using FTIR spectroscopy. The spectral data from the 400 – 4000 cm^{-1} range of wavenumbers demonstrate the formation of ZnO-CB NPs with an intense peak related to the (Zn–O) stretching vibrations at wavenumber 474 cm^{-1} , as has been previously reported in the literature (Thema et al., 2015). Other absorption peaks are primarily from the carboxylic groups apart from the hydroxyl functional groups like peaks at 1105 cm^{-1} assigned to C–O. Peaks at 2950 and 1400 cm^{-1} are assigned to stretching and bending vibrations of C–H bonds, respectively. The absorption peaks at 3444 and 1630 cm^{-1} are related to stretching (O–H) and bending (H–O–H) vibrations of adsorbed water molecules, respectively. Most likely, these peaks are from the byproducts of the burning of aqueous extract of non-edible parts of brinjal during the synthesis protocol (Thema et al., 2015).

3.1.3. UV-visible spectral analysis

Electronic band structure and band gap energy (E_g) are some of the key factors that determine the photocatalytic properties of a material (Dincer and Zamfirescu, 2016). Fig. 2A displays the UV-visible absorption spectrum of synthesized ZnO-CB NPs. The absorbance maximum is noticed around 352 nm; This is due to fundamental band-gap absorption, which is brought on by the electrical transition between the valence and conduction bands of Zn atoms, as has already been noticed ($O_{2p} \rightarrow Zn_{3d}$) (Zak et al., 2011). Kubelka-Munk theory (KMT) is applied to the absorption spectra data, and the direct band gap energy is calculated by plotting the transformed Kubelka-Munk function $(\alpha h\nu)^2$ on the Y-axis against the energy ($h\nu$) on the X-axis (Tauc plot).

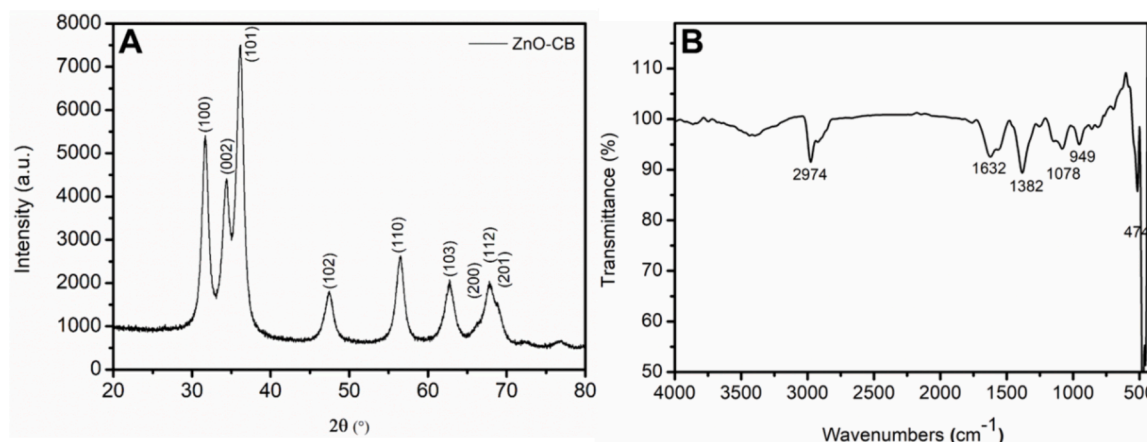


Fig. 1. (A) XRD pattern and (B) FTIR spectrum of the synthesized ZnO-CB NPs.

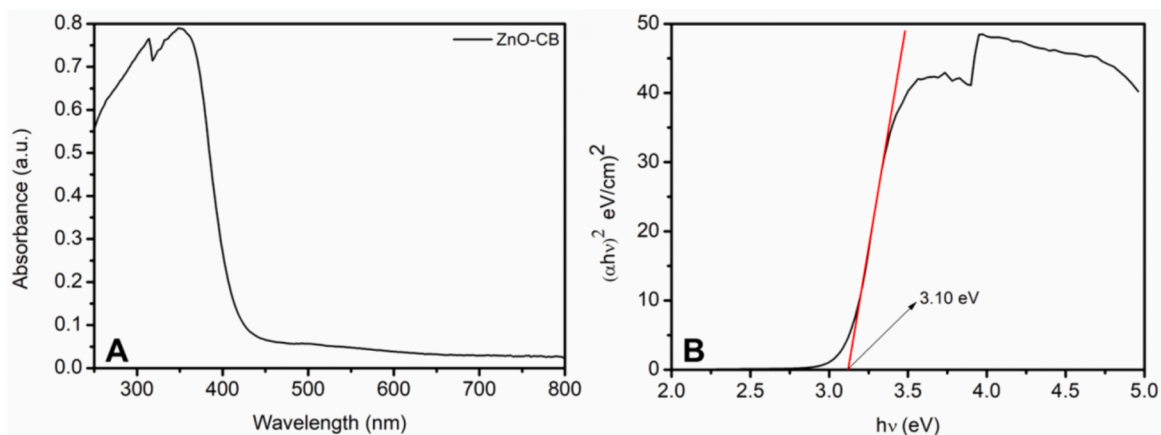


Fig. 2. (A) UV-Vis and (B) band gap spectra of the prepared ZnO-CB nanoparticles.

The direct bandgap energy of ZnO-CB NPs as they have been produced is anticipated to be 3.1 eV by extrapolating the straight line in the Tauc plot (Fig. 2B).

3.1.4. Morphological studies by SEM

Using SEM techniques, the morphological characteristics of the synthesized ZnO-CB NPs are assessed. Fig. 3A and 3B display the SEM images of ZnO-CB NPs at low and high magnifications. SEM images of the ZnO-CB NPs confirmed to have a porous structure on the surface with an irregular shape. The EDX analysis is carried out on the same sample, and the elemental composition is quantified (Fig. 3). The EDX

spectrum demonstrates that ZnO-CB NPs mostly contain the desired elemental composition, namely Zn and O, and the table inset displays their numerical percentage values.

3.2. Photocatalytic activity

3.2.1. Photocatalytic performance results of MG, BB1 and AO36 dyes over ZnO-CB NPs photocatalyst

The main objective of this study is to use green synthesized ZnO-CB NPs as a photocatalyst for the degradation of the hazardous MG, BB1, and AO36 dyes prevalent in the aqueous effluents of the textile industry.

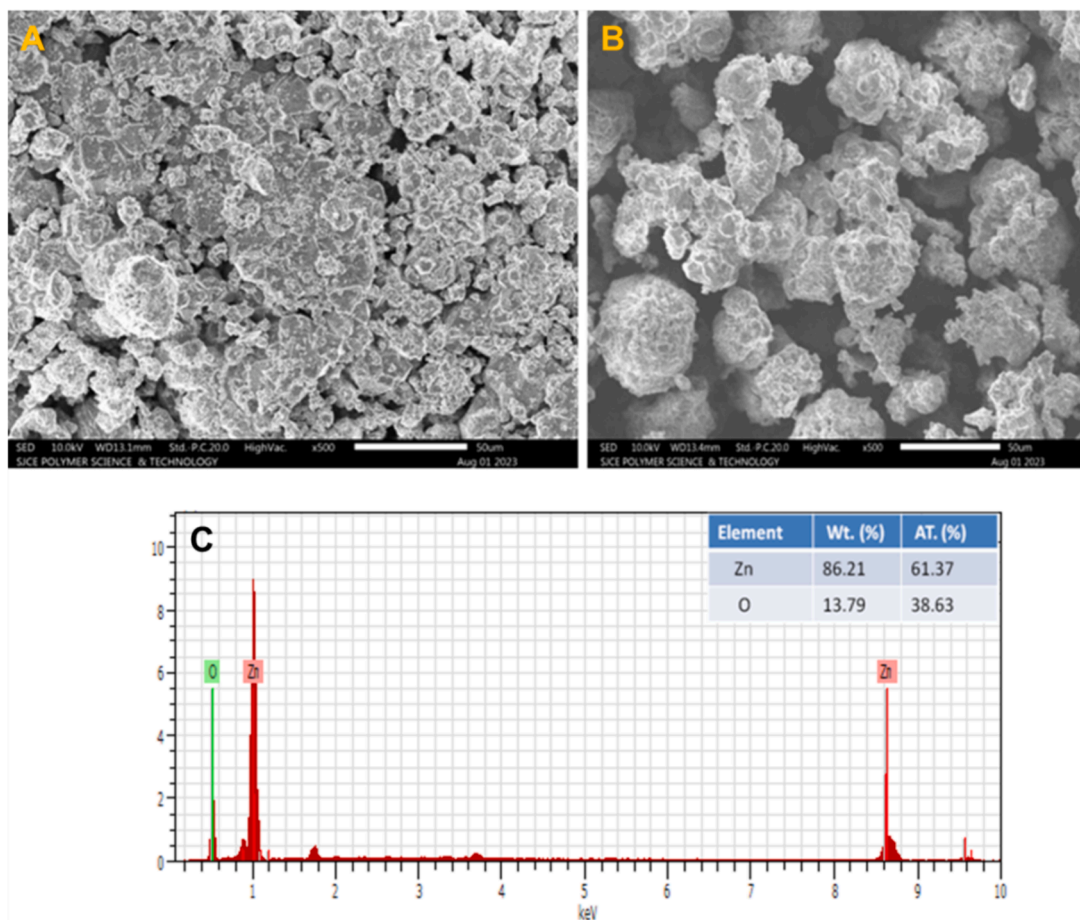


Fig. 3. (A) and (B) SEM micrographs of the fabricated ZnO-CB NPs. at different magnifications and (C) EDAX spectra of the prepared ZnO-CB NPs.

Various experimental setups are used to evaluate the photocatalytic degradation efficiency of the synthesized ZnO-CB NPs. The hypothesis states that the surface area, bandgap, crystallinity, particle size, morphology, and amounts of free OH radicals on the photocatalyst surface determine the photocatalytic activity of the semiconductor photocatalyst. The proposed model explained the formation of electrons and holes on the photocatalyst surface as a consequence of light absorption, along with the way these electrons and holes either take part in the process or proceed to recombination. If additional surfaces are made available for electrons and holes, they will migrate there and become trapped by hydroxyl radicals for the holes and a photocatalyst for the electrons, generating OH and HO₂. In order to efficiently employ the created hydroxyl radicals in dye photocatalytic degradation, photo-produced charge carriers have the opportunity to migrate on metal oxide nanoparticles due to the increased surface area (Kumar et al., 2021). The synthesized nanoparticles could absorb UV light and can have photo induced electronic transition as observed from the band value of 3.10 eV (calculated from Tauc plot) (Patil et al., 2018). The MG, BB1, and AO36 contaminants are chosen as the reference contaminants for photocatalytic degradation, and the study carefully evaluates the photocatalytic parameters of light source, photocatalyst quantity, dye concentration, pH value, and exposure period.

The initial and final dye concentrations (C_i & C_f) of the solution in the photocatalytic system are calculated from the UV-Vis spectra. By using the following Eq. (2), the degradation activity of the MG, BB1, and AY36 dyes is calculated

$$\text{Degradation}(\%) = \frac{C_i - C_f}{C_i} \times 100 \quad (2)$$

3.2.2. Influence of light source on dye decomposition

The initial research focuses on the effect of light sources for degrading the dyes with the greatest potential of the produced ZnO-CB NPs. Three different light sources—dark, UV light, and visible light—are employed in the studies to examine the effects of ZnO-CB NPs on the photocatalytic degradation of MG, BB1, and AO36 dyes. Fig. 4A(a–c) displays the photocatalytic results that are attained. To begin with, the degradation experiment is carried out in the dark, and all three dyes don't decay. Between the other two sources, the findings show that under UV light irradiation, the rate of photodecomposition of MG, BB1, and AO36 dyes is significantly higher than when experiments are carried out in the presence of visible light. The photocatalyst, ZnO-CB NPs,

under the irradiation of UV light, effectively promotes the degradation of all the 3 dyes in the starting minutes, as observed in Fig. 4A(a–c), even after 20 min. However, the degradation efficiency could not be visible in the presence of visible light or in the absence of any light source. The synthesized ZnO-CB efficiently degraded 99.3 % of MG, 99.6 % of BB1 in 100 min, and 99.5 % of AO36 in 120 min under UV light irradiation.

3.2.3. Influence of amount of ZnO-CB NPs photocatalyst on dye decomposition

The amount of catalyst indeed has some effects on the catalytic performance of any reaction. Herein, by increasing the amount of ZnO-CB NPs from 5.0 mg to 20.0 mg while maintaining a dye concentration of 6 ppm and a pH of 7 under UV light irradiation, a similar trend happened (Fig. 4B (d–f)). However, the catalytic efficacy is reduced after reaching the optimum level of active species. Only 77 % of MG dye degradation, 76 % of BB1, and 79 % of AO36 dye degradation are seen when 5.0 mg of photocatalyst is employed. The rates of degradation of MG, BB1, and AO36 are observed to be 88.6 %, 99.8 %, and 87 %, and 99.6 % and 90.0 %, and 99.5 %, respectively, when the photocatalyst dose is increased to 10.0 mg and later 15 mg. However, increasing the photocatalyst concentration to 20.0 mg led to a reduction in the degradation activity of MG dye (90 %), and rates are enhanced for both BB1 and AO36 dyes (Fig. 4B (d–f)).

The inclusion of more active sites in the medium, which can generate more radical ions, is directly responsible for the improvement in degradation. Due to the particle's surface energy, there will not be enough space for the nanoparticles to disperse in the solution when the photocatalyst dose exceeds a critical barrier, and the particles will adhere to each other and aggregate. As a result, the majority of photocatalytic active sites are blocked or covered up, lowering the system's degrading efficacy. As shown in Fig. 4B, all MG, BB1, and AO36 have the best degradation performance at 15.0 mg photocatalyst. However, the photocatalyst quantity variance is minor for all the dyes studied. As a result, 15.0 mg is chosen as the ideal photocatalyst dosage, which will be used in the remaining tests to optimize other variables.

3.2.4. Influence of dye concentration on dye decomposition

Alteration of the dye concentration from 3.0 ppm to 12.0 ppm under UV light irradiation while retaining the photocatalyst amount at 15.0 mg and pH 7 allows the assessment of the effects of dye concentrations in breaking down the MG, BB1, and AO36 dyes. The obtained results

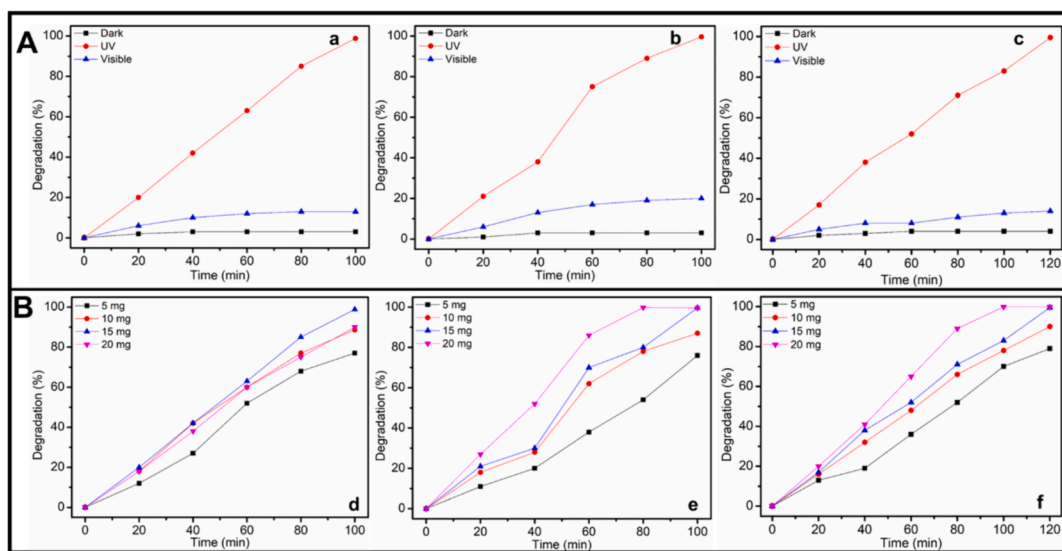


Fig. 4. Effect of (A) light source on photocatalytic degradation of (a) MG, (b) BB1 and (c) AO36 (Conditions: dye concentration = 6 ppm, photocatalyst amount = 15 mg, and pH of solution = 7) and (B) photocatalyst amount on photocatalytic decomposition of (d) MG (e) BB1 and (f) AO36 (Conditions: dye concentration = 6 ppm, pH of solution = 7, and UV light irradiation).

shown in Fig. 5 implicate that, under identical conditions, ZnO-CB NPs's photocatalytic activity is inversely related to the concentration of MG, BB1, and AO36 dyes, i.e., maximum removal efficacy is observed at lower concentrations (3 ppm). The photodegradation rate gradually dropped from 99.8 % to 77.5 % when the MG concentration increased from 3.0 to 12.0 ppm (Fig. 5A(a)). The same trend is observed with BB1 (99.9 % to 85.3 %–Fig. 5A(b)) and AO36 (99.9 %–86.4 %) with increased dye concentration from 3.0 to 12.0 ppm (Fig. 5A(c)). As dye concentration rises, light absorption on the photocatalyst surface decreases, limiting the production of $\text{OH}\cdot$ radical ions, which are crucial to the photodegradation process. Therefore, it is crucial to keep the ratio of photocatalyst to dye concentration constant. Consequently, for MG, BB1, and AO36, a dye concentration of 3.0 ppm yields the best photo-decomposition performance. Therefore, the dye concentration of 3.0 ppm has been decided upon for more optimization studies.

3.2.5. Influence of pH value on dye decomposition

The pH of the solution is, in fact, one of the most crucial factors in the photocatalytic decomposition of organic dyes, and the presence of $\text{OH}\cdot$ radicals in the reaction medium is frequently linked to the photocatalytic efficiency of the catalyst, which enhances dye photodegradation by several orders of magnitude in basic aqueous solutions. Fig. 5B(d–f) depicts the impact of pH solution on the photodegradation of MG, BB1, and AO36 dyes in the presence of ZnO-CB NPs. While maintaining all other variables constant, the impact of pH on the photodegradation of MG, BB1, and AO36 is examined at three different pH values of 4.0, 7.0, and 10.0. (i.e., 6.0 ppm concentration of dye, 15.0 mg catalyst amount, and UV light irradiation). At pH 4.0, where the percentage decomposition is at least 44, 47, and 45 percent of MG, BB1, and AO36, respectively, after 100 min.

However, as the pH of the solution rose, the ZnO-CB NPs photocatalyst showed higher degrading activity, with 99.3 %, 99.6 %, and 99.5 % at pH7 for MG, BB1, and AO36 respectively, and 99.99 % (almost 100 %) degradation of all the dyes at pH 10 (Fig. 5B(d–f)). This might be because higher pH values lead to the development of negative charges on the photocatalyst surface. Since all three dyes studied, MG, BB1, and AO36, are positively charged cationic dyes, they have absorbed on the surface. Additionally, higher pH levels promote the deposition of additional $\text{OH}\cdot$ radical ions on the photocatalyst surface, which enhances the efficiency of the photodegradation process.

The photodegradation rates for ZnO-CB NPs towards the chosen

organic dyes are calculated using the pseudo-first-order Langmuir–Hinshelwood (L-H) kinetic model (Akpan and Hameed 2009) through the following Equations (3):

$$r = \frac{dC}{dt} = kC \quad (3)$$

where r – oxidation rate of the chosen dye, C –concentration of chosen dye, t – radiation exposure time in minutes, and k – the pseudo-first-order reaction rate constant (min^{-1}).

Finally, by transforming Equation (3) through integration and converting it into natural logarithmic form, the rate constant can be obtained from the slope of the following linear Equation (4):

$$\ln(C_i/C_f) = kt \quad (4)$$

Fig. 6 calculates the first-order degradation rate constant of ZnO-CB NPs for the degradation of dyes such as MG, BB1, and AO36. The rate constant for the degradation of MG is found to be 0.00529, 0.04326, and 0.03099 min^{-1} for pH 4, 7, and 10, respectively. Similarly, 0.00618, 0.04654, and 0.10556 min^{-1} and 0.00526, 0.0354, and 0.07124 min^{-1} for BB1 and AO36 at pH 4, 7, and 10, respectively.

A comparison of the photo-decomposition performance of the synthesized ZnO-CB NPs photocatalyst with many formerly reported photocatalytic systems containing ZnO for the removal of the organic dyes is displayed in Table 1. The prepared ZnO-CB NPs photocatalyst has superior photo-degradation performance for MG, BB1, and AO36 dyes under UV light irradiation.

3.2.6. Photocatalytic mechanism

The possible method for the photocatalytic degradation of the MG/BB1/AO36 dye on the ZnO-CB surface is depicted in Scheme 1B. The electron-hole pairs form between the valence band (VB) and conduction band (CB) of ZnO-CB NPs when exposed to UV light. As a result, oxygen scavenges the photo-produced electrons (e^-) in the ZnO-CBNPs to form an anion radical (O_2^-), which, upon protonation yields $\text{HOO}\cdot$. Despite the less, the photoinduced holes (h^+) produced by the VB of ZnO-CB will react with the ^-OH group or H_2O to produce highly reactive species of OH^- ions. As a result, the dye degradation is caused by the generated OH^- radical ions, which subsequently form less toxic byproducts like H_2O and CO_2 . As a result, the harmful pollutant MG/BB1/AO36 dye is broken down by OH^- and h^+ active species and a potential process is illustrated below.

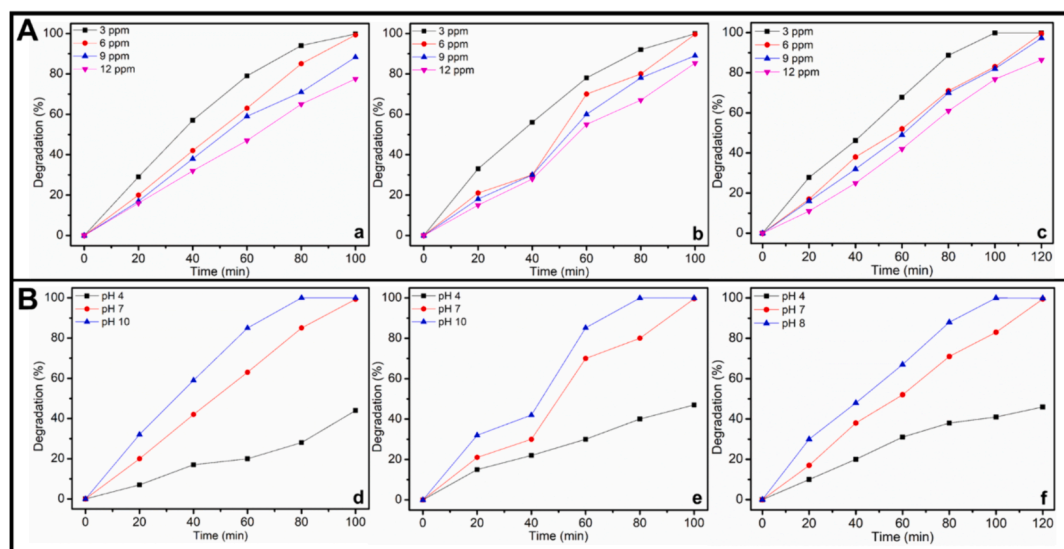


Fig. 5. Effect of (A) concentration of dye on photocatalytic decomposition of (a) MG, (b) BB1 and (c) AO36 (Conditions: photocatalyst amount = 15 mg, pH of solution = 7, and UV light irradiation) and pH of solution on photocatalytic degradation of (d) MG, (e) BB1 and (f) AO36 (Conditions: dye concentration = 6 ppm, photocatalyst amount = 15 mg, and UV light irradiation).

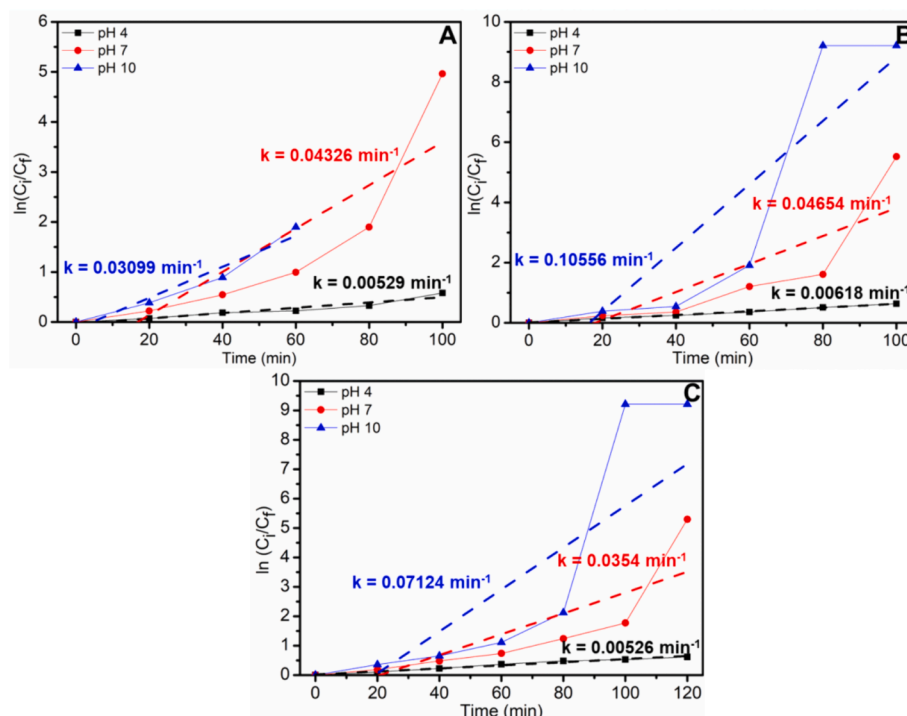


Fig. 6. Kinetics data of photocatalytic degradation of (A) MG, (B) BB1, and (C) AO36 under different pH using ZnO-CB NPs photocatalyst (conditions: dye concentration = 6 ppm, photocatalyst amount = 15 mg, and UV light irradiation).

Table 1

Comparison of photodecomposition efficacy of ZnO-CB NPs with other previously published analogues photocatalysts for degradation of MG, BB1 and AO36 dyes.

Catalyst	Dye	Light Source	Time (min)	Degradation (%)	Reference
SnO ₂ /ZnO	Malachite green	Visible	150	98	(Zhang et al., 2022)
ZnO/chitosan	Methylene blue	Visible	5	96	(Mostafa et al., 2020)
ZnO	Methylene blue	UV	100	60	(Khalid et al., 2023)
ZnO	Eriochrome Black T	Fluorescent black	30	99.6	(Lanjwani et al., 2023)
ZnO-[5%]WO ₃	Methyl Orange	Sunlight	120	100	(Ashiegbu and Potgieter 2023)
ZnO	Rhodamine B	UV	70	95	(Lal et al., 2023)
Ag/ZnO	Indigo carmine	Visible	120	95.7	(Kumar et al., 2023)
ZnO	Methyl Orange	UV	180	76.3	(Al-Mamun et al., 2023)
Cu/ZnO	Methyl Orange	UV	180	81.9	(Al-Mamun et al., 2023)
Cu/Ni/ZnO	Methyl Orange	UV	180	83.4	(Al-Mamun et al., 2023)
ZnO/ACTTS	Methyl orange	UV	90	66.8	(Machrouhi et al., 2023)
ZnO-CB	MB	UV	100	99.3	Herein
	BB1		100	99.6	
	AO36		120	99.5	



According to the aforementioned equations the photo-decomposition of dye is accomplished over the ZnO-CB NPs photocatalyst.

3.2.7. Reusability of ZnO-CB NPs

The utilized ZnO-CB NPs are treated and used for the degradation of

MG, BB1, and AO36 dyes under identical conditions as in detailed studies. The used photocatalyst is calcined at 300 °C and reused for the degradation of all dyes studied at the optimized condition of 15 mg catalyst, 6 ppm dye under pH 7 with the illumination of UV light. ZnO-CB NPs showed performance as shown in the by Fig. 7. It can be observed that upon the first time reuse, there is a slight depreciation of catalytic activity, however upon reactivation of the catalyst and reusing it for the second time, the results revealed that there is a significant depreciation in catalytic performance.

3.3. Studies on the performance of ZnO-CB NPs as additives for biodiesel blends

3.3.1. Experimental setup and procedure

The performance and emission tests are carried out as our previous study (Kavalli et al., 2022). The performance tests are carried out on a Kirloskar TV1 four-stroke-single-cylinder, water-cooled compression ignition engine. An eddy current dynamometer is used for engine loading. Sensors are placed at required junctions to calculate the

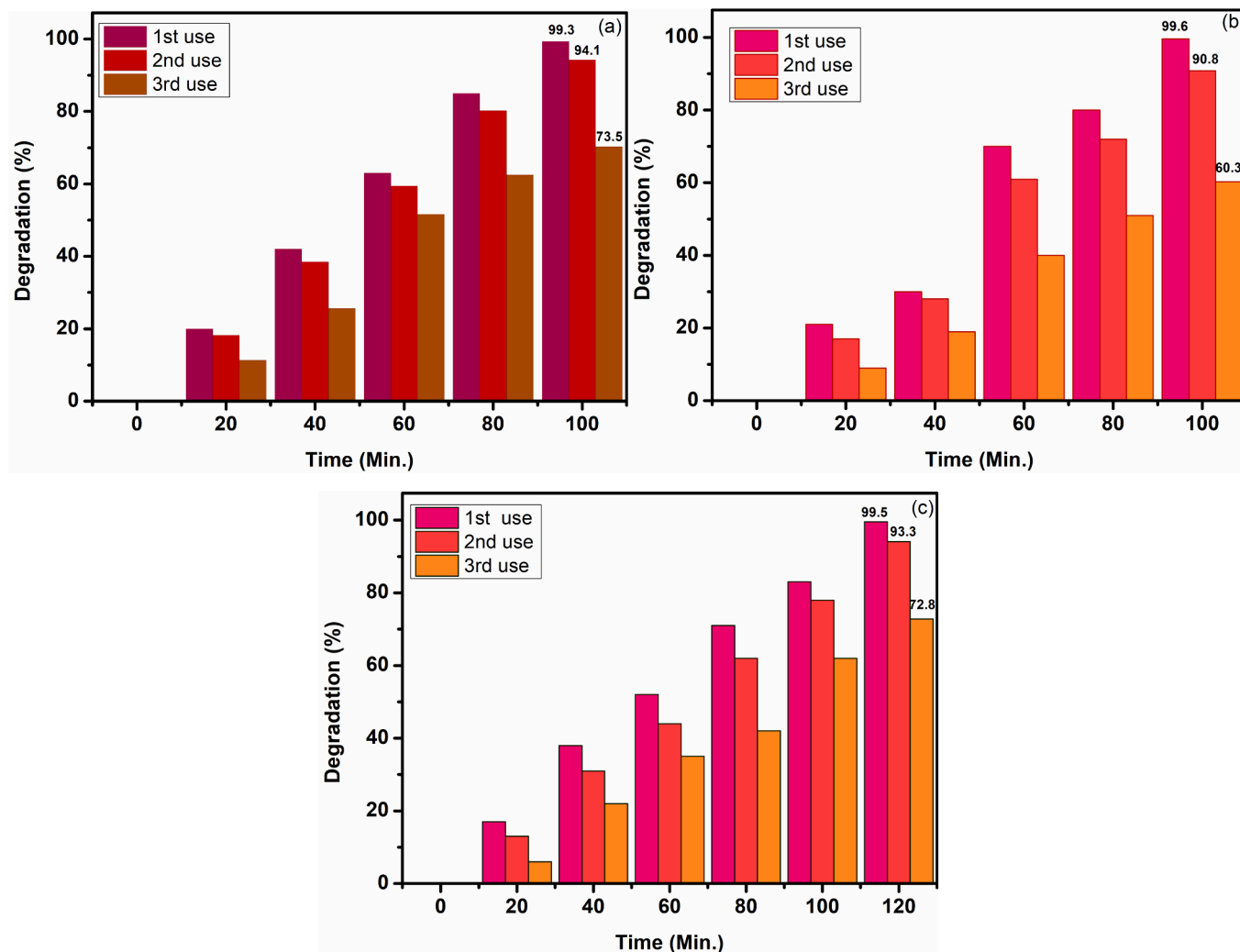


Fig. 7. Reusability of ZnO-CB NPs for the photocatalytic degradation of MG, BB1, and AO36 dyes under identical conditions over a period of 2 h.

temperatures. A rotameter is used for measuring the engine jacket water and cooling water flow rates. An Indus exhaust gas analyzer is used for measuring emission parameters.

3.3.2. Brake thermal efficiency (BTHE) and brake-specific fuel consumption (BSFC) analysis

The impact of the blend MPME20 and the MPME20 blend with ZnO-

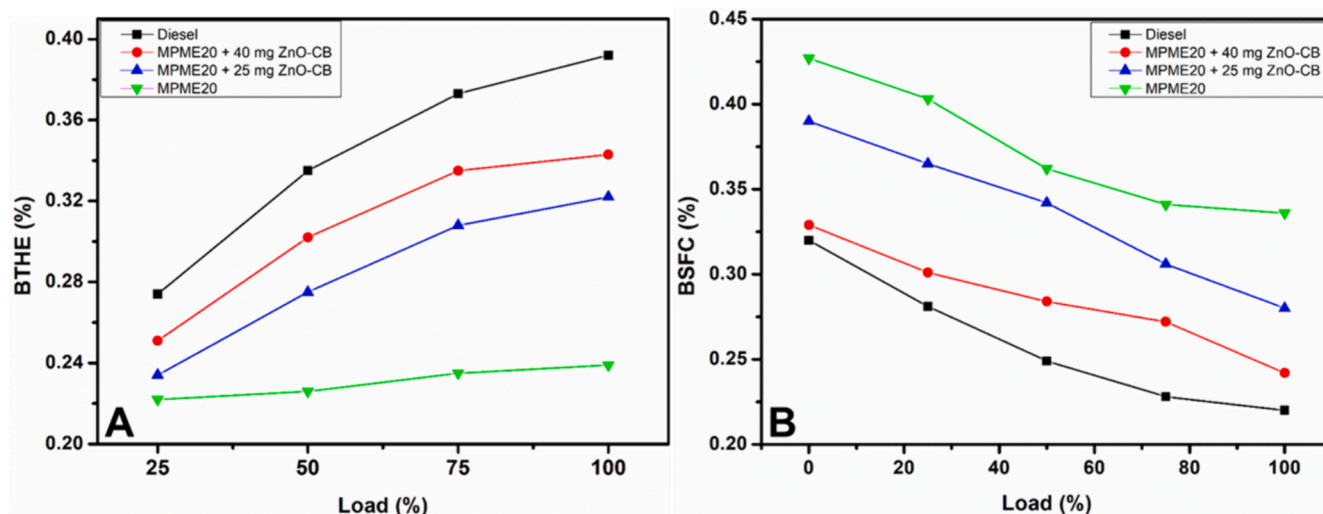


Fig. 8. Graphical illustration of (A) brake thermal efficiency (BTHE) and (B) brake-specific fuel consumption from diesel and blends vs. load (%). MPME20, MPME20 + 25 mg ZnO-CB; MPME20 + 40 mg ZnO-CB.

CB nanoparticles, i.e., MPME20 + 25 mg ZnO-CB and MPME20 + 40 mg ZnO-CB, on the engine performance, such as brake thermal efficiency (BTHE) and brake specific fuel consumption (BSFC), is analyzed. The values obtained from the analysis carried out are shown in Fig. 8. Significant improvements in the fuel competence of the blend MPME20 are observed when MPME20 is further blended by changing the amount of ZnO-CB NPs; moreover, the blend with 40 mg, i.e., MPME20 + 40 mg ZnO-CB, displays the best fuel efficiency but is not comparable to commercial diesel. The dosage of ZnO-CB from 25 mg to 40 mg shifts the performance of biodiesel towards diesel.

The improved heat transport character, resulting in a faster combustion process, and elevated oxygen content assist the entire combustion of fuel, resulting in higher efficiency, which can be accredited to the role played by the ZnO-CB NPs due to an increase in surface area of the crystallite size of ZnO-CB nanoparticles. Furthermore, the brake-specific fuel consumption (BSFC) values for the blends indicate the engine performance characteristics required for converting fuel consumption to work (Fig. 8B). It can be seen that the fuel consumption is higher with blend B20 when compared to commercial diesel; however, adding varying amounts of ZnO-CB NPs to the blend MPME20, can reduce the brake-specific fuel consumption (BSFC) values significantly. This could be because of higher oxygen content or reduced ignition delay that enhances the combustion properties. The improved combustion efficiency leads to an increase in the fuel momentum and fuel propagation, resulting in cloud-like emulsified moisture during the injection.

3.3.3. Carbon monoxide (CO) emission

Carbon monoxide emitted from the diesel engine may be due to fuel

combustion in a shorter time and less availability of oxygen. It is found that commercial diesel yielded 0.09 % of CO, while blended B20 yielded 0.08 %. However, in the blends with ZnO nanoparticles, i.e., MPME20-25 mg ZnO-CB and MPME20-40 mg ZnO-CB, the ZnO-CB NPs performed as oxygen-donating catalysts. They improved the oxidation of CO, which is evident with the 0.068 % and 0.066 % of CO obtained, respectively. The metallic ZnONPs are found to be favourable concerning their effects on emission reduction and engine performance enhancement. The graphical illustration of the results obtained is given in Fig. 9A.

3.3.4. Carbon dioxide (CO₂) emission

As observed from the previous study, the blends with ZnO-CB NPs yielded lower CO emissions. However, the studies of the impact of ZnO-CB NPs blended concentration in B20 on the emission of CO₂ reveal that the blends with higher ZnO-CB NPs yield an increase in CO₂ emission; this could be due to the complete combustion of hydrocarbons and CO, which produces carbon dioxide and water as combustion products. An amount of 9.1 % of CO₂ is obtained from the use of commercial diesel, while 13.7 % of CO₂ is obtained from the use of MPME20 + 40 mg ZnO-CB. The increased concentration of carbon dioxide in emissions also indicates the lesser emission of carcinogenic carbon monoxide by converting it into carbon dioxide due to the presence of ZnO-CB NPs in the blend MPME20, which acts as an oxidizing agent. ZnO-CB. Moreover, it can be said that the addition of nanoparticles results in a reduced ignition delay period, enhanced calorific value, and oxidation rates, leading to a complete and cleaner combustion. The pictorial representation emission pattern obtained is plotted in Fig. 9B.

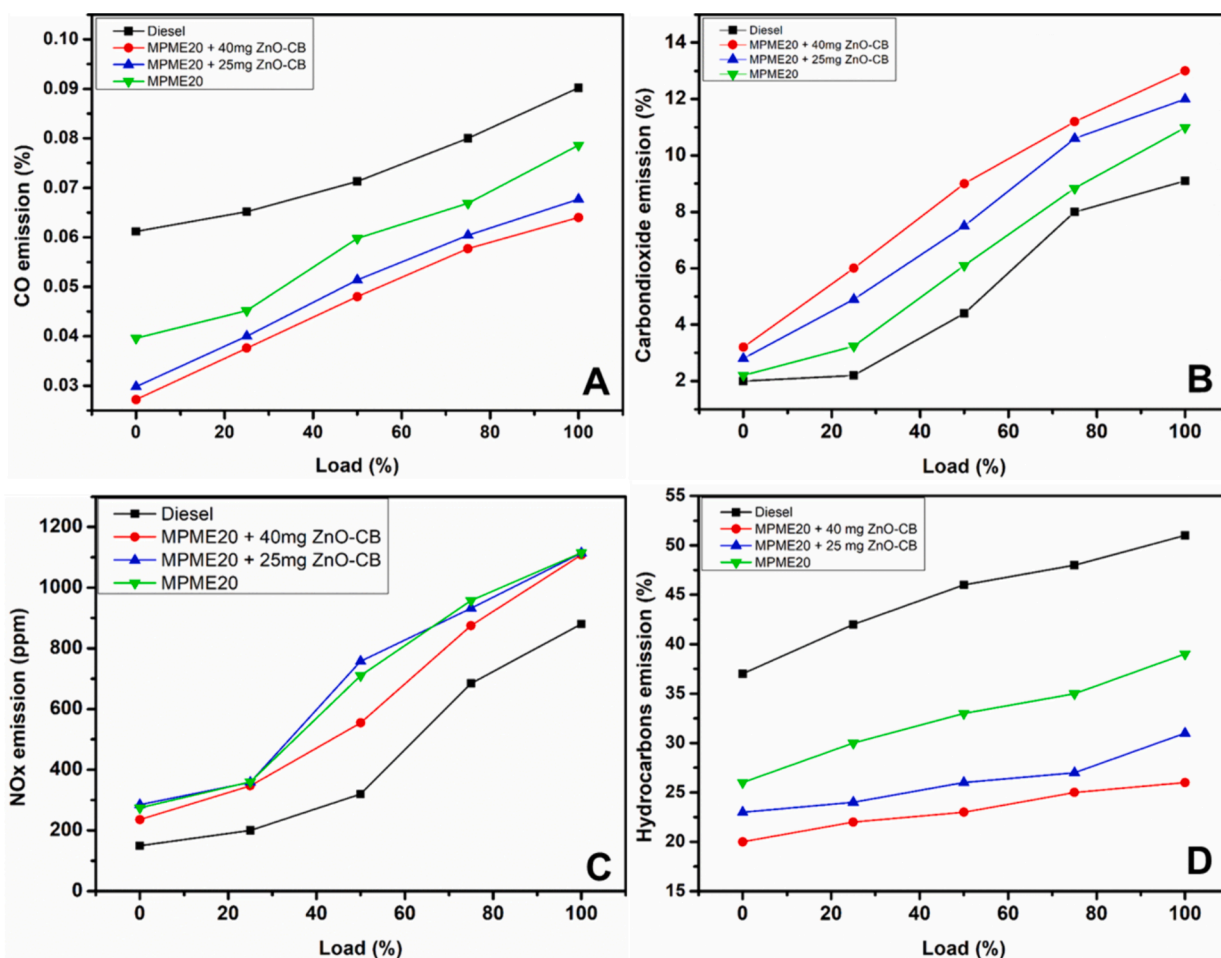


Fig. 9. Graphical illustration of (A) carbon monoxide, (B) carbon dioxide, (C) nitrogen oxide and (D) hydrocarbon emissions from diesel and blends vs. load (%). MPME20, B20 + 25 mg ZnO-CB; MPME20 + 40 mg ZnO-CB.

3.3.5. Nitrogen oxide (NO_x) emission

The presence of nitrogen compounds, together with elevated oxygen content and combustion chamber temperature, is what causes fuels to emit NO_x. Because of its effects on the environment and human health, nitrogen oxide (NO_x) emissions are a serious concern. Acid rain, smog, air pollution, and a number of respiratory problems are all caused by NO_x molecules, especially nitrogen dioxide (NO₂) and nitric oxide (NO). Vehicle catalytic converters frequently use zinc oxide (ZnO) to lower NO_x emissions. Adsorption of NO_x on the catalyst surface is the first step in the process, after which it is reduced to nitrogen (N₂) and oxygen (O₂). ZnO is an active ingredient in the catalyst that facilitates this reaction. The process by which ZnO reduces NO_x entails multiple steps: (1) Adsorption: The ZnO surface is adsorbent to NO_x molecules. A few examples of the variables that affect this adsorption process are temperature, catalyst characteristics, and gas composition. (2) Surface reactions: NO_x molecules are adsorbed and then interact with other molecules on the catalyst surface. The creation of intermediate species and the transport of electrons are involved in these reactions. (3) Reduction: Innocuous nitrogen and oxygen compounds are the result of the reduction of intermediate species that arise during surface reactions. For NO_x emissions to be properly reduced, this reduction method is necessary. (4) Regeneration: The catalyst requires renewal on a periodic basis in order to remain active. This may entail procedures such as the oxidation of leftover chemicals or the desorption of accumulated species. Particle size, surface area, catalyst composition, and operating conditions are some of the variables that affect how well ZnO reduces NO_x emissions. To reduce NO_x as much as possible while maintaining maximum efficiency, these settings must be optimized. In general, creating effective catalytic systems to reduce NO_x emissions and enhance air quality requires a thorough understanding of the intricate chemical interactions between NO_x and ZnO.

Blended MPME20 produces 1108 parts per million of NO_x emissions, far greater than commercial diesel (880 parts per million). Nevertheless, it has been discovered that adding more ZnO-CB NPs, specifically MPME20 + 25 mg and MPME20 + 40 mg, slightly reduces NO_x emissions to 1114 ppm and 1117 ppm, respectively. This may be because of the advanced catalytic effect, affirmative effect, and shorter combustion times, which convert NO_x to simple nitrogen (Fig. 9C).

3.3.6. Hydrocarbon (HC) emission

Partial combustion of fuel fragments is the cause of hydrocarbon (HC) emissions from fuels. It is revealed that commercial diesel produces 51 % HC, while the MPME20 blend produces 39.4 % HC. ZnO NPs can be added to MPME20 to create blends of MPME20 + 25 mg ZnO-CB and MPME20 + 40 mg ZnO-CB, which can significantly lower the amount of HC emission to as much as 26 % and 31 %, respectively. The catalytic activity of ZnO-CB, which permits the full oxidation of the HC in the fuel fragments, may be the cause of the decrease in HC emission. Fig. 9D provides a graphical representation that is comparable.

4. Conclusions

In summary, ZnO-CB NPs are efficiently synthesized through an environmentally benign, low-cost, straightforward, and one-step combustion method using calyxes of brinjal. The highly pure form hexagonal ZnO-CB nanoparticles are confirmed using different types of characterization techniques such as XRD, UV-vis, FTIR, SEM, and EDX techniques. The as-synthesized ZnO-CB NPs have been used for the photocatalytic decomposition of MG, BB1, and AO36 dyes as toxic industrial pollutants. The results promised excellent catalytic performance in the degradation of the aforementioned dyes. The optimization of the catalytic performance was carried out by varying the source of light, photocatalyst quantity, concentration of dye, and pH of medium over a period of 2 h with sample analysis in 20 min intervals. The as-synthesized photocatalyst showed commendable photocatalytic efficacy (>99 %) of MG, BB1, and AO36 dyes in 120 min at the optimum

circumstances. It is remarkable to note that the outstanding photo-elimination performance of ZnO-CB NPs for the degradation of dyes is mainly accredited to electron-hole separation generated on the surface of the photocatalyst through UV irradiation. ZnO-CB NPs also showed better performance in reducing harmful emissions from automobile exhaust. The inexpensive, environment-friendly, and highly competent ZnO-CB NPs with photocatalytic characteristics can be considered an ideal material for wastewater treatment and related photocatalytic applications. The heterogeneous blend of MPME20, which was created by blending 25 mg of as-prepared ZnO-CB NPs, significantly decreased greenhouse gas emissions while also increasing fuel efficiency, according to emission studies. In conclusion, it can be said that MPME20 + 25 mg ZnO-CB can be utilized to boost brake thermal efficiency without endangering the engine's performance and without causing any operating difficulties.

Funding

The authors acknowledge the financial support provided by the Researchers Supporting Project number (RSPD2024R665), King Saud University, Riyadh, Saudi Arabia.

CRediT authorship contribution statement

J.P. Shubha: Writing – review & editing, Writing – original draft, Supervision. **B. Roopashree:** Formal analysis, Data curation. **N.V. Sushma:** Formal analysis, Data curation. **K. Kiran:** Investigation, Formal analysis. **R. Ravikumar:** Methodology, Investigation. **Mufsir Kuniyil:** Methodology, Formal analysis. **Mohammed Rafi Shaik:** Funding acquisition, Formal analysis. **Mujeeb Khan:** Writing – review & editing. **Syed Farooq Adil:** Writing – review & editing, Writing – original draft, Project administration.

Declaration of competing interest

The authors declare that they have no known competing financial interests or personal relationships that could have appeared to influence the work reported in this paper.

Acknowledgments

The authors acknowledge the funding from Researchers Supporting Project number (RSPD2024R665), King Saud University, Riyadh, Saudi Arabia.

References

- Abbasi, B.A., Iqbal, J., et al., 2019. Plant-mediated synthesis of nickel oxide nanoparticles (NiO) via *Geranium wallichianum*: characterization and different biological applications. *Mater. Res. Express* 6 (8), 0850a0857.
- Akpan, U.G., Hameed, B.H., 2009. Parameters affecting the photocatalytic degradation of dyes using TiO₂-based photocatalysts: a review. *J. Hazard. Mater.* 170 (2), 520–529.
- Alharthi, F.A., Al-Zaqri, N., et al., 2020. Synthesis of nanocauliflower ZnO photocatalyst by potato waste and its photocatalytic efficiency against dye. *J. Mater. Sci. Mater. Electron.* 31 (14), 11538–11547.
- Al-Mamun, M.R., Iqbal Rokan, M.Z., et al., 2023. Enhanced photocatalytic activity of Cu and Ni-doped ZnO nanostructures: a comparative study of methyl orange dye degradation in aqueous solution. *Heliyon* 9 (6), e16506.
- Amin, S., Tahira, A., et al., 2019. A sensitive enzyme-free lactic acid sensor based on NiO nanoparticles for practical applications. *Anal. Methods* 11 (28), 3578–3583.
- Ampah, J.D., Yusuf, A.A., et al., 2022. Progress and recent trends in the application of nanoparticles as low carbon fuel additives—a state of the art review. *Nanomaterials* 12. <https://doi.org/10.3390/nano12091515>.
- Ashiegbu, D.C., Potgieter, H.J., 2023. ZnO-based heterojunction catalysts for the photocatalytic degradation of methyl orange dye. *Heliyon* 9 (10), e20674.
- Attar, A., Yapaoz, M.A., 2018. Biomimetic synthesis, characterization and antibacterial efficacy of ZnO and Au nanoparticles using echinacea flower extract precursor. *Mater. Res. Express* 5 (5), 055403.
- Belver, C., Bedia, J., et al., 2019. Chapter 22 - semiconductor photocatalysis for water purification. In: Thomas, S., Pasquini, D., Leu, S.-Y., Gopakumar, D.A. (Eds.), *Nanoscale Materials in Water Purification*. Elsevier, pp. 581–651.

- Bououdina, M., Azzaza, S., et al., 2017. Structural and magnetic properties and DFT analysis of ZnO:(Al, Er) nanoparticles. *RSC Adv.* 7 (52), 32931–32941.
- Capek, I. 2006. Chapter 1 Nanotechnology and nanomaterials. In: *Studies in Interface Science*. I. Capek, Vol. 23. Elsevier, pp. 1–69.
- Desantes, J., Molina, S., et al., 2020. Comparative global warming impact and NOX emissions of conventional and hydrogen automotive propulsion systems. *Energy Convers. Manage.* 221, 113137.
- Devarajan, Y., Munuswamy, D.B., et al., 2019. Investigation on behavior of diesel engine performance, emission, and combustion characteristics using nano-additive in neat biodiesel. *Heat Mass Transf.* 55 (6), 1641–1650.
- Di, T., Xu, Q., et al., 2019. Review on metal sulphide-based Z-scheme photocatalysts. *ChemCatChem* 11 (5), 1394–1411.
- Dincer, I., Zamfirescu, C., 2016. Chapter 5 - hydrogen production by photonic energy. Elsevier, pp. 309–391.
- Dooley, K.M., Chen, S.Y., et al., 1994. Stable nickel-containing catalysts for the oxidative coupling of methane. *J. Catal.* 145 (2), 402–408.
- Elumalai, P., Balasubramanian, D., et al., 2021. An experimental study on harmful pollution reduction technique in low heat rejection engine fuelled with blends of pre-heated linsed oil and nano additive. *J. Clean. Prod.* 283, 124617.
- Esfes, M.H., Arani, A.A.A., et al., 2018. Improving engine oil lubrication in light-duty vehicles by using of dispersing MWCNT and ZnO nanoparticles in 5W50 as viscosity index improvers (VII). *Appl. Therm. Eng.* 143, 493–506.
- Fosso-Kankeu, E., Pandey, S., et al., 2020. Photocatalysts in Advanced Oxidation Processes for Wastewater Treatment. John Wiley & Sons.
- Hasannuddin, A., Yahya, W., et al., 2018. Nano-additives incorporated water in diesel emulsion fuel: fuel properties, performance and emission characteristics assessment. *Energy Convers. Manage.* 169, 291–314.
- Hassaan, M.A., El Nemr, A., et al., 2017. Testing the advanced oxidation processes on the degradation of Direct Blue 86 dye in wastewater. *Egypt. J. Aquat. Res.* 43 (1), 11–19.
- Javed, S., Murthy, Y.S., et al., 2016. Effect of a zinc oxide nanoparticle fuel additive on the emission reduction of a hydrogen dual-fuelled engine with jatropa methyl ester biodiesel blends. *J. Clean. Prod.* 137, 490–506.
- Karaköse, E., Çolak, H., 2018. Structural, electrical, and antimicrobial characterization of green synthesized ZnO nanorods from aqueous *Mentha* extract. *MRS Commun.* 8 (2), 577–585.
- Kavalli, K., Hebbur, G.S., et al., 2022. Green synthesized ZnO nanoparticles as biodiesel blends and their effect on the performance and emission of greenhouse gases. *Molecules* 27. <https://doi.org/10.3390/molecules27092845>.
- Khalid, A., Ahmad, P., et al., 2023. Structural, optical, and renewable energy-assisted photocatalytic dye degradation studies of ZnO, CuZnO, and CoZnO nanostructures for wastewater treatment. *Separations* 10 (3), 184.
- Kumar, T.D., Hussain, S.S., et al., 2020. Effect of a zinc oxide nanoparticle fuel additive on the performance and emission characteristics of a CI engine fuelled with cotton seed biodiesel blends. *Mater. Today: Proc.* 26, 2374–2378.
- Kumar, R., Janbandhu, S.Y., et al., 2023. Visible light assisted surface plasmon resonance triggered Ag/ZnO nanocomposites: synthesis and performance towards degradation of indigo carmine dye. *Environ. Sci. Pollut. Res.* 30 (44), 98619–98631.
- Kumar, M.S.S., Soundarya, T.L., et al., 2021. Multifunctional applications of Nickel oxide (NiO) nanoparticles synthesized by facile green combustion method using *Limonia acidissima* natural fruit juice. *Inorg. Chim. Acta* 515, 120059.
- Lal, M., Sharma, P., et al., 2023. Photocatalytic degradation of hazardous Rhodamine B dye using sol-gel mediated ultrasonic hydrothermal synthesized of ZnO nanoparticles. *Result. Eng.* 17, 100890.
- Lanjwani, M.F., Khuhawar, M.Y., et al., 2023. Photocatalytic degradation of eriochrome black T dye by ZnO nanoparticles using multivariate factorial, kinetics and isotherm models. *J. Clust. Sci.* 34 (2), 1121–1132.
- Lavand, A.B., Malghe, Y.S., 2015. Visible light photocatalytic degradation of 4-chlorophenol using C/ZnO/CdS nanocomposite. *J. Saudi Chem. Soc.* 19 (5), 471–478.
- Machrouhi, A., Khiar, H., et al., 2023. Synthesis, characterization, and photocatalytic degradation of anionic dyes using a novel ZnO/activated carbon composite. *Watershed Ecol. Environ.* 5, 80–87.
- McCormick, R.L., Williams, A., et al., 2006. Effects of Biodiesel Blends on Vehicle Emissions: Fiscal Year 2006 Annual Operating Plan Milestone 10.4. National Renewable Energy Lab.(NREL), Golden, CO (United States).
- Mills, A., Davies, R.H., et al., 1993. Water purification by semiconductor photocatalysis. *Chem. Soc. Rev.* 22 (6), 417–425.
- Mostafa, M.H., Elsayy, M.A., et al., 2020. Microwave-assisted preparation of chitosan/ZnO nanocomposite and its application in dye removal. *Mater. Chem. Phys.* 248, 122914.
- Narendra Kumar, H.K., Chandra Mohana, N., et al., 2019. Phyto-mediated synthesis of zinc oxide nanoparticles using aqueous plant extract of *Ocimum americanum* and evaluation of its bioactivity. *SN Appl. Sci.* 1 (6), 651.
- Natarajan, S., Bajaj, H.C., et al., 2018a. Recent advances based on the synergetic effect of adsorption for removal of dyes from waste water using photocatalytic process. *J. Environ. Sci.* 65, 201–222.
- Natarajan, T.S., Thampi, K.R., et al., 2018b. Visible light driven redox-mediator-free dual semiconductor photocatalytic systems for pollutant degradation and the ambiguity in applying Z-scheme concept. *Appl. Catal. B* 227, 296–311.
- Navarro, P., Gabaldón, J.A., et al., 2017. Degradation of an azo dye by a fast and innovative pulsed light/H2O2 advanced oxidation process. *Dyes Pigm.* 136, 887–892.
- Padalia, H., Baluja, S., et al., 2017. Effect of pH on size and antibacterial activity of *Salvadora oleoides* leaf extract-mediated synthesis of zinc oxide nanoparticles. *BioNanoScience* 7 (1), 40–49.
- Patil, S.B., Ravishankar, T.N., et al., 2018. Multiple applications of combustion derived nickel oxide nanoparticles. *J. Mater. Sci. Mater. Electron.* 29 (1), 277–287.
- Pirhashemi, M., Habibi-Yangjeh, A., et al., 2018. Review on the criteria anticipated for the fabrication of highly efficient ZnO-based visible-light-driven photocatalysts. *J. Ind. Eng. Chem.* 62, 1–25.
- Pouretedal, H.R., Norozi, A., et al., 2009. Nanoparticles of zinc sulfide doped with manganese, nickel and copper as nanophotocatalyst in the degradation of organic dyes. *J. Hazard. Mater.* 162 (2–3), 674–681.
- Prabu, A., Anand, R., 2016. Emission control strategy by adding alumina and cerium oxide nano particle in biodiesel. *J. Energy Inst.* 89 (3), 366–372.
- Rajak, U., Nageswara Reddy, V., et al., 2023. Modifying diesel fuel with nanoparticles of zinc oxide to investigate its influences on engine behaviors. *Fuel* 345, 128196.
- Singh, J., Dutta, T., et al., 2018. 'Green' synthesis of metals and their oxide nanoparticles: applications for environmental remediation. *J. Nanobiotechnol.* 16 (1), 84.
- Soudagar, M.E.M., Mujtaba, M., et al., 2021. Effect of Sr@ZnO nanoparticles and Ricinus communis biodiesel-diesel fuel blends on modified CRDI diesel engine characteristics. *Energy* 215, 119094.
- Soudagar, M.E.M., Nik-Ghazali, N.-N., et al., 2020. An investigation on the influence of aluminium oxide nano-additive and honge oil methyl ester on engine performance, combustion and emission characteristics. *Renew. Energy* 146, 2291–2307.
- Suhel, A., Abdul Rahim, N., et al., 2023. Impact of ZnO nanoparticles as additive on performance and emission characteristics of a diesel engine fueled with waste plastic oil. *Heliyon* 9 (4), e14782.
- Supraja, N., Prasad, T., et al., 2016. Synthesis, characterization, and evaluation of the antimicrobial efficacy of *Boswellia ovalifoliolata* stem bark-extract-mediated zinc oxide nanoparticles. *Appl. Nanosci.* 6 (4), 581–590.
- Thema, F.T., Manikandan, E., et al., 2015. Green synthesis of ZnO nanoparticles via *Agathosma betulina* natural extract. *Mater. Lett.* 161, 124–127.
- Thovhogi, N., Park, E., et al., 2016. Physical properties of CdO nanoparticles synthesized by green chemistry via *Hibiscus Sabdariffa* flower extract. *J. Alloys Compd.* 655, 314–320.
- Yusuf, S.N.A., Sidik, N.A.C., et al., 2020. A comprehensive review of the influences of nanoparticles as a fuel additive in an internal combustion engine (ICE). *Nanotechnol. Rev.* 9 (1), 1326–1349.
- Zak, A.K., Razali, R., et al., 2011. Synthesis and characterization of a narrow size distribution of zinc oxide nanoparticles. *Int. J. Nanomed.* 6, 1399–1403.
- Zhang, Y., Liu, B., et al., 2022. Synthesis of SnO₂/ZnO flowerlike composites photocatalyst for enhanced photocatalytic degradation of malachite green. *Opt. Mater.* 133, 112978.
- Zollinger, H., 2003. *Color Chemistry: Synthesis, Properties, and Applications of Organic Dyes and Pigments*. John Wiley & Sons.